Received: 23 October 2023 | Revised: 21 December 2023 | Accepted: 21 December 2023 | Published online: 12 January 2024

RESEARCH ARTICLE

Journal of Optics and Photonics Research
2024, Vol. 00(00) 1–9
DOI: 10.47852/bonviewJOPR42021933

BON VIEW PUBLISHING

Sensitivity Analysis of SPR Nanohole Array Structure for Lab-On-Chip Application

Suryanarayana N K[1,3], Venkatesha Muniswamy[1,3,*] and Asha K[2,3]

[1]*Department of Electronics and Communication Engineering, Sai Vidya Institute of Technology, India*

[2]*Department of Electronics and Communication Engineering, BMS Institute of Technology and Management, India*

[3]*Department of Electrical and Electronic Sciences, Visvesvaraya Technological University, India*

Abstract: In this work, sensitivity analysis of surface plasmon resonance-based nanohole array (SPR NHA) is reported. SPR NHA are suitable for lab-on-a-chip applications. These devices work in three different modes, namely intensity mode, phase mode, and angular mode. In this work, intensity mode analysis is used. The SPR NHA consisting of gold metal and silicon dioxide substrate dielectric material is used. Gold material is widely used in SPR sensors due to its excellent optical properties, high electrical conductivity, and biocompatibility. The finite difference time domain method is used for the simulation and analysis. An optical source at a wavelength of 675 nm is used for the analysis and simulation. The structure of the proposed SPR NHA consists of substrate, which is made of silicon di oxide dielectric material, and a thin layer of gold is deposited on the substrate having thickness 0.1 μm. The NHA is etched on the gold layer. The pitch of the NHA is 0.6 μm and diameter of each hole is 0.2 μm. The diameter of the holes present in NHA is 0.2 μm. The sensitivity of the proposed device for different analytes such as albumin, RBC, and hemoglobin is determined. The maximum sensitivity of 298.35 nm/RIU is achieved for the proposed device. The results obtained show that the sensor has better sensitivity and suitable for use in lab-on-a-chip applications.

Keywords: nanohole array (NHA), SPR, finite difference time domain, sensitivity, surface plasmons

1. Introduction

Surface plasmon resonance (SPR) is a phenomenon observed at the interface of metal and dielectric. The two configurations used in surface plasmon (SP) waves are Otto and Kretschmann. The finite difference time domain (FDTD) is the mathematical modeling method used to find the field intensity and spatial distribution of the SPR sensor structure [1, 2]. Prism couplers, grating couplers, and waveguide couplers are commonly used devices in SPR [3]. SPs are the continuous oscillating waves generated at the metal dielectric surface. Gold and silver nanoparticles are commonly used materials in SPR sensors. Diffraction-based optical gratings are mainly used in SPR biosensors. Nanohole arrays (NHAs) are fabricated on the gold surface as self-assembled monolayers. This 4 × 4 microarray sensor was tested with a 50% alcohol solution in water and a 20% alcohol solution in water for protein microarray detection. An experiment was conducted for the detection of solution concentration. The 8 mm × 8 mm area is divided into a 4 × 4 array [4]. Nano disk exhibits magneto-optical effects that have localized SPR (LSPR) [5]. SPR is used in imaging technology, where a single-flow cell reaction is monitored. Biomolecular interactions can be monitored with a SPR imaging tool [6]. The dipole coupling phenomenon of SPR leads to narrow peaks. The biomolecular interaction was measured with the help of the following devices: Biacore's Flex chip, Plexera's Proteomic Processor, and many more. The antibodies are readily available, and they are used in agglutination tests. These tests are used in ABO blood typing [7]. Slit array nano plasmonic devices on thin metal films show the coupling between the SP modes and excited states [8]. SP polaritons are observed when dipole–dipole coupling is used [9].

NHAs are sub-diffraction optical devices with good transmission, and they observe the high electric field intensity in the UV-visible spectrum. The three-dimensional FDTD time domain technique was used to calculate the optical transmission properties of NHA [10]. The different sensor designs include the following: SPR, LSPR, micro-cantilever SPR sensor, grating-coupled interferometer sensor, waveguide interferometer sensor, resonance waveguide sensor, reverse symmetry sensor, metal-clad waveguide sensor, and metal-clad waveguide sensor [11]. The Kretschmann geometry is used to find the resonant shift [12]. Metal-hole arrays have extraordinary optical transmission (EOT) and act as resonators. SP lasing phenomenon was observed in the metal hole arrays. The work reported [13] shows that a single mode is needed to understand the dispersion of the luminescence maxima. An array or group of nanoholes on the gold films were fabricated, and the light transmission spectra of incident white light were analyzed [14]. This article uses a discrete dipole approximation. The UV-visible spectrum is used in the experimentation process. Atomic force microscopy (AFM) was used to explain a polystyrene nanosphere-based array with silver nanoparticles [15]. Chromium (Cr) metal is used as a SPR NHA [16]. The lithography process is used for the fabrication of a periodic array of silver nanoparticles. The different

*Corresponding author: Venkatesha Muniswamy, Department of Electronics and Communication Engineering, Sai Vidya Institute of Technology, India and Department of Electrical and Electronic Sciences, Visvesvaraya Technological University, India. Email: venkatesha.m@saividya.ac.in

methods that are used in the fabrication of SPR sensors are AFM and scanning electron microscopy (SEM) [17]. Nano disk fabrication uses the electron beam lithography (EBL) process [5]. The EBL process is used to fabricate the photonic nanoarrays. There are different sizes and shapes of arrays, namely circular, hexagonal, and rectangle. Nano plasmonic and microfluidics go hand in hand and have many applications in the medical industry [18]. Subwavelength hole arrays were fabricated using quartz and silver film materials using the focused ion beam (FIB) method. The transmission spectra depend on the hole period, which in turn changes the photon energy, which is measured in electron volts (eV) [19]. Optical metallic nano slits are the sensing elements used in the article [20].

The nano plasmonic devices with nano pillar and nano ring are used for sensitivity improvement and SPR-based biosensing [21]. Self-assembled colloidal lithography is used for the fabrication of tunable metallic nanodevices. Polystyrene sphere arrays were fabricated with different diameters. The interparticle spacing is adjusted by using O2 plasma treatment [22]. Nanoholes are more popular nanodevices used in SPR sensors. EOT to NHA SPR sensing, the author has considered two materials, such as bare gold and coated gold. The transmission spectra of the NHA with two different materials fabricated were analyzed [23]. The detection limit of the adsorbed film-based SPR is 0.003 nm [24]. In applications such as chemical analysis of certain substances, deoxyribonucleic acid (DNA) sequencing, and biochemical modeling, this technology is used. Glucose measurement in blood and counting the infected cell numbers in the blood are a few examples [25] used. LOC is used in the detection of DNA hybridization. Specific DNA sequences are analyzed to verify the DNA mutations. Ribonucleic acid (RNA), protein synthesis, and DNA are other measurements taken using the device. Poly dimethyl siloxane is used to fabricate the flow cell used in the microfluidic system. SPR chips are fabricated using the lithography process. RNA chips, protein chips, and DNA chips are fabricated, and experimentation is carried out [26]. In many LOC devices, normalized reflection versus wavelength was measured. LPSR and surface acoustic wave are two concepts used in LOC [27].

Label-free bio detection is a technology where sensing uses optics to convert biological signals into electrical signals. The methods of detection are in vivo and in vitro. Structural color filter-based NHA is used in marker-free detection; this originated from LSPR [28]. Plasmonic base gold NHA chip was fabricated. The images of SEM show the clear and perfect image of the gold NHA [29]. Human blood group detection is explained in the elliptical NHA. The sensitivity values are measured [30]. Ring-shaped gold nanoparticles were fabricated. The gold (Au) nanohole array (ANA)-based Ag NPs are used for fluorescence [31]. Nano pore arrays are part of plasmonic devices. Fabrication of gold (metal), anodic aluminum oxide (media metal), and gold (metal) nanopore arrays is explained in this article [32]. FIBs and e-beam lithography were the fabrication methods. The main applications of SPR sensors are in the detection of chemical and biological species. These are used to measure food quality and safety analysis [33]. SPR is used in bio sensing applications; the evanescent wave of SPR detects the bio-analyte binding on the thin receptor films on the sensor surface. The SPR interferometry method was utilized in microarray bio sensing applications [34]. Metallic nano-slits are used to implement the sensitive biosensor. Attenuated total reflection (ATR) is the methodology used in glass prisms; the sensitivity measured is 400 nm/RIU. These biosensors are used in protein microarray and DNA chip-based detections [35]. The SPR sensors are used to monitor protein interaction and DNA hybridization [36]. In this work, the range of refractive index (RI) used in this article is 1.333–1.364 RIU [37].

From the literature work, it is concluded that SPR-based biosensors are used for accurately detect molecule interactions at the nanoscale, and NHAs are extremely important for biosensing applications. These nanostructures provide extremely sensitive, real-time biomolecular binding event monitoring, which is an essential tool for understanding biological processes and diagnosing diseases. SPR-based NHAs' special optical characteristics increase signal sensitivity, which makes them essential for developing biosensor technologies that enable quick and precise identification of a variety of biomolecules. Overall, SPR sensors are used in LOC applications and point-of-care diagnostic applications as a biosensor.

The further sections in this article are organized as follows: Section 2 describes the mathematical modeling of the proposed SPR NHA. Simulation and analysis of SPR NHA are discussed in Section 3. The sensitivity of the proposed SPR NHA is discussed in Section 4.

2. Mathematical Modeling of Proposed SPR NHA

This section gives detailed mathematical modeling of the proposed SPR NHA. The propagation constant of SPR is given by Equation (1) below [33].

$$\beta_{SP} = \frac{\omega_0}{C}\sqrt{\frac{\varepsilon_d \varepsilon_m}{\varepsilon_d + \varepsilon_m}} \tag{1}$$

where $\frac{\omega_0}{C} = k_0$ is the wave number, ε_m and ε_d are the metal relative permittivity and dielectric permittivity, respectively, ω_0 is the frequency of plasmon, and C is the propagation velocity in vacuum.

In the Kretschmann configuration, the ATR phenomenon is used. In this configuration, the surface component of a photon's wave vector is given by Equation (2) [6].

$$k_{ATR} = \frac{\omega}{c}\sin\theta\sqrt{\varepsilon_p} \tag{2}$$

where ε_p is the prism dielectric constant, and θ is the light wave angle of incident.

The wavelength of the SPR wave is given by the formula shown in Equation (3). This equation holds good for square NHAs [10].

$$\lambda = \frac{P}{\sqrt{i^2 + j^2}}\sqrt{\frac{\varepsilon_m}{\varepsilon_d + \varepsilon_m}} \tag{3}$$

where P is the periodicity of the array, and variables "i" and "j" are resonance integer indices.

The permittivity of metal (the gold layer) is described using the Lorentz–Drude model, as shown in Equation (4) [10].

$$\varepsilon(\omega) = \varepsilon_\infty + \sum_0^M \frac{f_m \omega_p^2}{\omega_m - \omega^2 + i\omega\Gamma_m} \tag{4}$$

where ε_∞ is the permittivity in the infinite frequency, ω is the incident frequency, ω_p is the gold plasm frequency, and m^{th} resonance frequency is represented as ω_m. Γ_m is the m^{th} damping frequency.

Table 1
SPR nanohole array sensor

Layer name	Materials	Refractive index
Substrate	Silicon di oxide (SiO_2))	1.45
Thin film	Gold (Au)	Depicted in Figure 1 (n,k) as a function of wavelength
Nanohole array	Air	1

Table 1 shows the SPR NHA material and corresponding RI values. Figure 1 shows the perspective view of the proposed SPR NHA. The substrate material is the silicon dioxide, and the thin film is made of gold material. The NHA is created on the gold thin film layer, which is obtained by etching or creating air-filled holes on the gold material.

Gold has excellent optical properties and biocompatibility, and it also exhibits SPR properties. Gold offers high electrical conductivity compared to other metals such as silver, copper, and aluminum. The RI values of the gold material with respect to wavelength are plotted. The index of gold simulated is shown in Figure 2. Gold metal gives a SPR signal at a particular wavelength. Gold is a chemically inert material for other solutes and biochemicals.

The diameter of the holes present in NHA is 0.2 μm. The hole radius is 0.1 μm. The substrate material for the simulation of the SPR NHA is the silicon dioxide having length of 2.5 μm in x-direction, width of 1 μm in y-direction, and height of 0.5 μm in z-direction. SPR NHA thickness is 0.1 μm.

Figure 2 shows the prospective view of the proposed SPR NHA. The time signal waveform of the applied light source is shown in Figure 3. The spectrum of the time signals with respect to wavelength lambda is shown in Figure 4. A plane wave source with a wavelength of 400–750 nm is applied. The type of plane wave source is Bloch or periodic [38]. For an electron moving at a periodic potential if the period of potential is a, then potential is $V(x+a) = V(x)$.

The Schrodinger equation is shown in Equation (5).

$$\frac{h^2}{2m}\frac{d^2\psi}{dx^2} + V(x)\psi = E\psi \tag{5}$$

The Bloch theorem states that the propagating wave will be in the form shown in Equation (6).

$$\psi = e^{ikx}u_k(x) \tag{6}$$

where k is the wave propagation along two directions. ψ is the eigen-state of the single electron Hamiltonian.

3. Simulation and Analysis of SPR NHA

This section gives detailed simulation settings and intensity mode profile analysis of the proposed SPR NHA. The working principle of SPR sensors is the interaction of the SPs, dielectric, and metal medium due to changes in the RI. SPR sensors are classified into different modes. The first one is angular mode.

Figure 1
The proposed SPR NHA structure. (a) Perspective view. (b) 2D view of NHA. (c) Perspective view of NHA

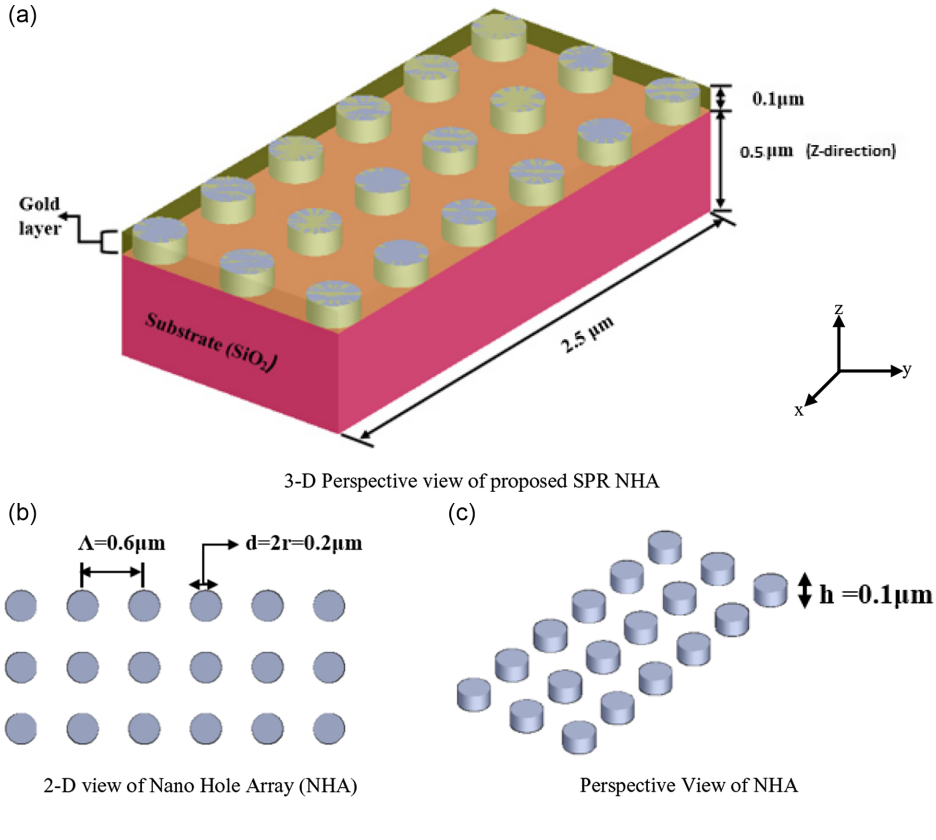

3-D Perspective view of proposed SPR NHA

2-D view of Nano Hole Array (NHA)

Perspective View of NHA

Figure 2
Refractive index (RI) of gold as a function of wavelength (*n*: real value of RI and *k*: imaginary value of RI)

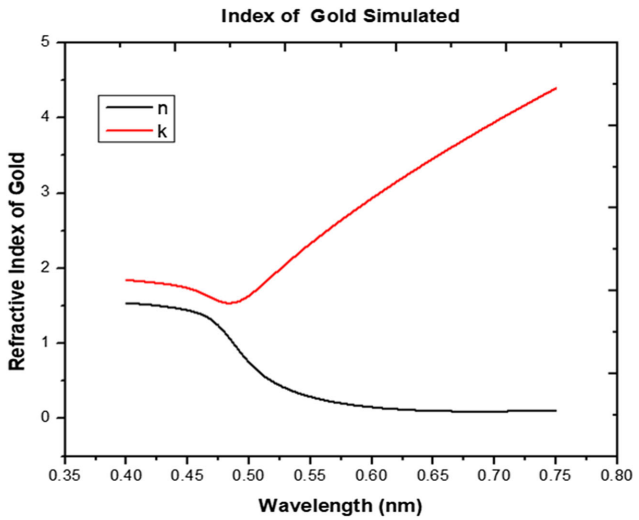

Figure 3
Time signal of the applied light source

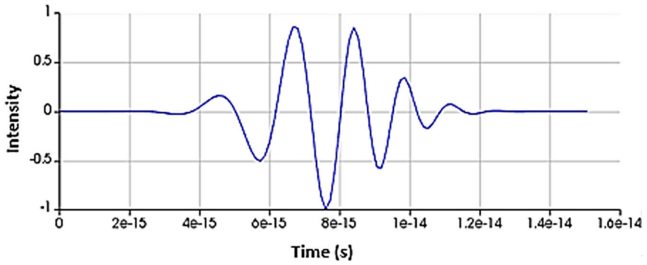

Figure 4
Spectrum of the applied light source

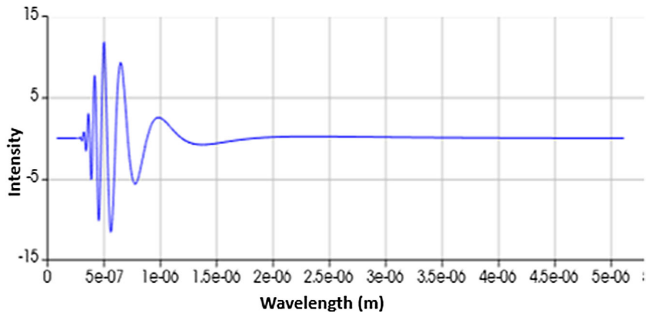

Here, the angle of incidence of the sensor is varied to excite SPs, and a shift in the wavelength is also measured. The second is the wavelength mode, where a polychromatic light source is used to excite the sensor and a corresponding change in the wavelength is measured. The third mode is the phase mode. In the phase mode, the shift in the phase is measured by maintaining the wavelength and angle constant. In intensity mode, wavelength and incident angle are kept constant, and reflected or transmitted light is measured [33]. In the proposed model, intensity mode analysis is used for further analysis and calculations. The intensity mode analysis is calculated, and the transmittance spectrum, reflectance spectrum, and *XY* plane spectrum are analyzed.

3.1. Simulation settings

The FDTD modeling method is used in this work. A three-dimensional structure is simulated with a time of 500 fs. Stretched boundary conditions perfectly matched layer (PML) is used in the modeling of SPR NHA as shown in Table 2. Anti-symmetric boundary conditions are initialized from *X* minimum to maximum. *Y* minimum to maximum uses the symmetric boundary conditions. PML boundary conditions are used from *Z* minimum to maximum.

Table 2
Stretched coordinate PML boundary conditions

Boundary conditions	Values
Layer	12
Kappa	3
Sigma	1.5
Polynomial	3
Minimum layers	12
Maximum layer	64
Alpha	0
Alpha polynomial	1

3.2. Intensity mode profile analysis

Intensity mode is used in analyzing the SPR NHA sensor. When the device is modeled and simulated, the frequency domain field monitors are used to get the different field profiles of the result.

Variational FDTD method is used as a mathematical modeling technique. Field profiles and power monitors are applied to obtain the different graphs, namely electric field data with respect to position, magnetic field data with respect to position, and Poynting vector values with respect to position. There are different types of modes in the SPR sensor calculation. The three modes of analysis are intensity mode, phase mode, and angular mode. Intensity mode analysis is implemented. The sensitivity is calculated using the intensity mode spectrum. These obtained graphs are shown in Figures 4, 5, and 6, respectively, for transmission, reflectance, and the *xy* plane.

The transmittance profile at 675 nm is shown in Figure 5. This transmission profile has three fields, namely the electric field, whose peak value is 6.8 arbitrary units (a.u.), the magnetic field, whose peak value is 0.0124 arbitrary units, and the Poynting vector field, whose peak value is 0.0418 arbitrary units with respect to position, as shown in Figure 5. Reflectance profile is shown in Figure 6. It has an electric field intensity of 11.6 arbitrary unit peak value, a magnetic field intensity of 0.0231 arbitrary unit peak value, and a Poynting vector field with the highest intensity of 0.105 arbitrary unit peak value. The *XY* plane profile is shown in Figure 7. The electric field has the highest intensity of 10.7 arbitrary units, the magnetic field has an amplitude of 0.0231, and the Poynting vector has an amplitude of 0.0872 arbitrary units.

4. Results and Discussions

In this section, the sensitivity of the proposed SPR NHA is calculated based on RI-based sensing. The resonant wavelength of various analytes with amplitude and RI is listed in Table 3. The

Figure 5
Transmittance profile. (a) E-field. (b) H-field. (c) Power density

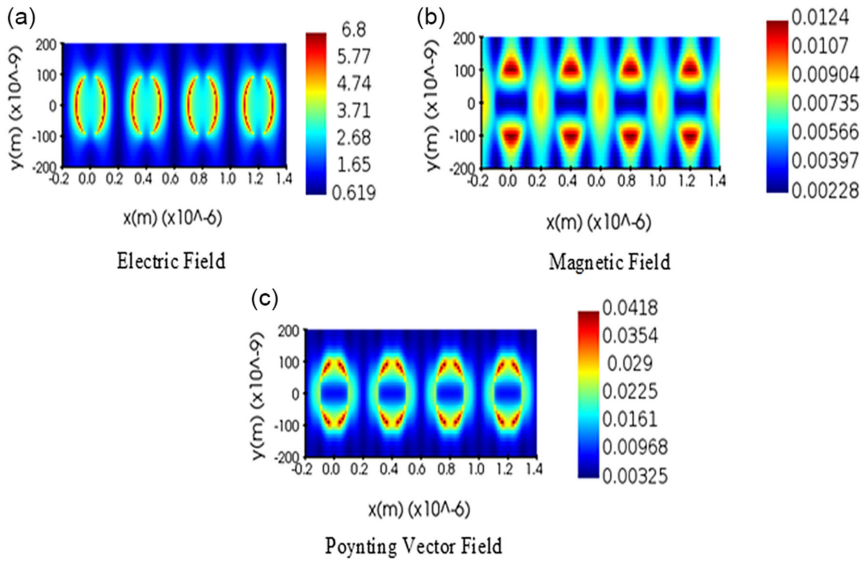

Figure 6
Reflectance profile. (a) E-field. (b) H-field. (c) Power density

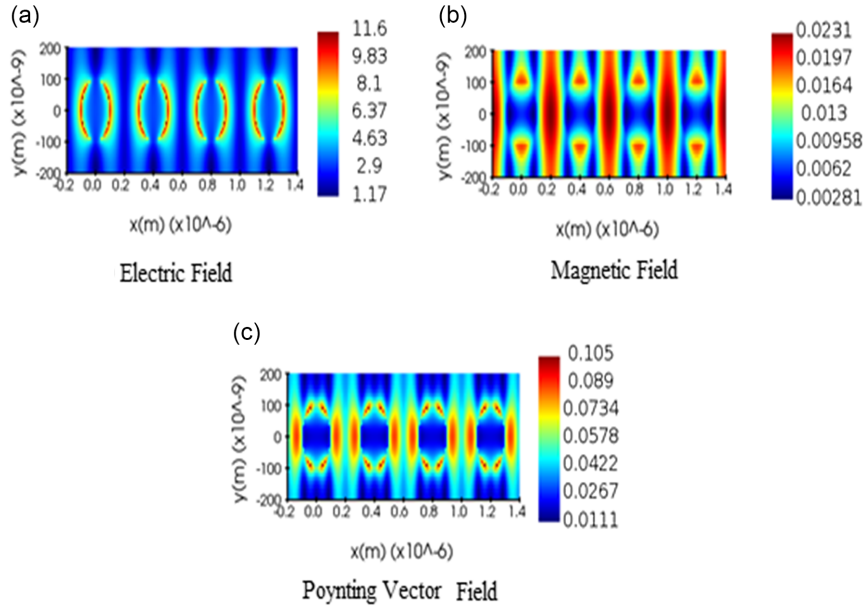

RI values are measured at the 680 nm wavelength. The RI of air, albumin solution in water, and RI hemoglobin solution in water are listed in the table below. The FDTD mathematical modeling method is used in the simulation.

The shift in the SPR sensor is due to changes in the effective dielectric constants at the interface of the metal and dielectric layer. This process is because of molecular adsorption. By using a weighted average within the changed interface, the effective dielectric constant may be calculated. The I_d of the evanescent SP mode's expansion into the dielectric (z direction) is given in Equation (7) [24].

$$\varepsilon_{eff} = \frac{2}{I_d}\int_0^{\infty} \varepsilon(z)\exp\left(-\frac{2z}{I_d}\right) dz \tag{7}$$

Figure 8 displays the transmission spectra for different RI values of the analytes. A change in the RI of the analyte results in a modification of

Figure 7
Field distribution plots (2D). (a) E-field intensity plot. (b) Magnetic field intensity plot. (c) Power density (W/m^2) plot

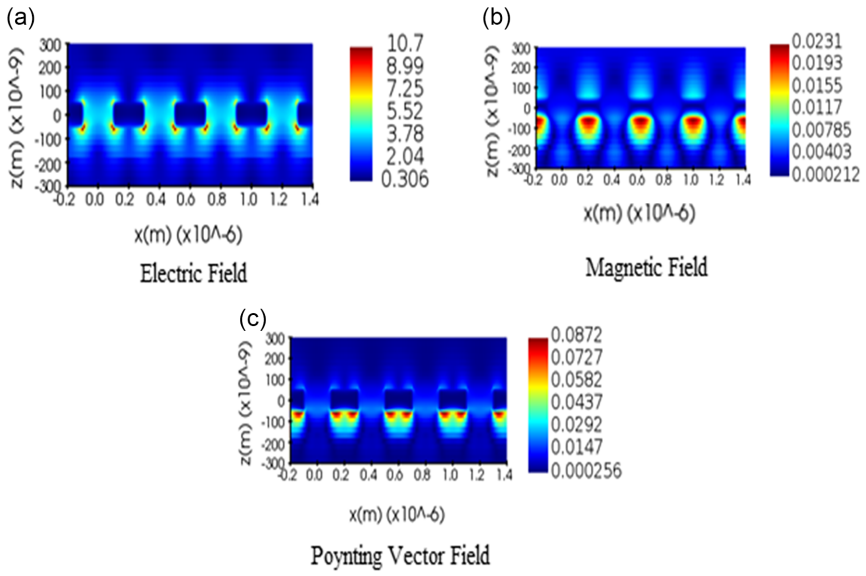

Table 3
Refractive index values for different analyte and resonant wavelength

Bio analyte	Refractive index (n)	Amplitude	Resonant wavelength
RI of air	1	0.81267	629.798
RI of albumin solution in water (55g/l)	1.3405	0.85071	636.869
RI of blood	1.3600	0.85380	640.404
RI of hemoglobin solution in water (260g/l)	1.3837	0.85651	647.475

The RI values are from Lazareva & Tuchin [39].

the resonant wavelength shift, which can be observed, and it is used for the calculations of sensitivity as a function of wavelength.

The transmitted light intensity is represented (Equation (8)) by knife edge cuts using a Gaussian beam that move towards the x axis [15]

$$T(x) = \frac{1}{2}\left[1 + erf\left(\frac{\sqrt{2}(x - x_0)}{w}\right)\right] \tag{8}$$

where T(x) is the power transmission, knife position is denoted as, w is the radius of the beam, and erf is the error function. The transmission spectrum shows the values of normalized transmission for different RI. Figure 9 is the normalized transmission spectrum; the highest peaks of amplitudes are observed at different wavelengths. The wavelength shift occurs as there is a change in the RI. SPR NHA wavelength change can be approximated by the formula given in Equation (9) [35].

$$\Delta\lambda = \lambda_1 - \lambda_2 \sim \left(\sqrt{\varepsilon_{s_1}} - \sqrt{\varepsilon_{s_2}}\right) = \mathrm{P}\Delta n \tag{9}$$

where Δn is the refractive index change. The normalized transmission spectrum of SPR NHA is shown in Figure 9. The sensor has to have the following parameter: sensitivity, low cost, scalability, high stability, limit of detection, and ease of use. To sustain and compete with other types of sensors in the market, the parameters play a very important role. The sensitivity values obtained are comparable with the article, designing of nano slit array [35]. The sensitivity obtained is comparable with the results of different designs of nanodevice [14].

The sensitivity is given by Equation (10) [11]. The sensitivity of the SPR NHA changes according to the variation in the RI of the surrounding medium, which is nearer to the device at a particular wavelength.

$$S = \frac{\Delta\lambda}{\Delta n} = \frac{P}{\sqrt{i^2 + j^2}}\sqrt{\left(\frac{\varepsilon_m}{\varepsilon_d + \varepsilon_m}\right)^3} \tag{10}$$

where $\Delta\lambda$ is the wavelength shift in the plasmon resonance and Δn is the change in the RI. In perforated metal film, P is the lattice constant (nanohole distance), and i and j are non-zero integers; they represent the 2D array scattering order.

Table 4 shows the resonant wavelength with amplitude, sensitivity, and RI values. It is concluded that the highest sensitivity of 298.35 nm/RIU is achieved for an analyte having RI of 1.36, which is almost close to RI of human blood. Such sensors can be used to detect various pathological parameters present in blood for detection of various diseases. Based on the simulation for different analyte values, the amplitude values are obtained for the analyte sample at a particular wavelength as

Table 4
Resonant wavelength and sensitivity of various analytes

RI value	Maximum amplitude (a.u)	Wavelength (nm)	Sensitivity (nm/RIU)
1	0.81267	629.798	20.77
1.3405	0.85071	636.869	181.28
1.3600	0.8538	640.404	298.35
1.3837	0.85651	647.475	–

Figure 8
Transmission spectrum for different values of refractive index (RI) of analytes (1 (air), 1.3405 (albumin), 1.36 (blood), and 1.3837 (hemoglobin))

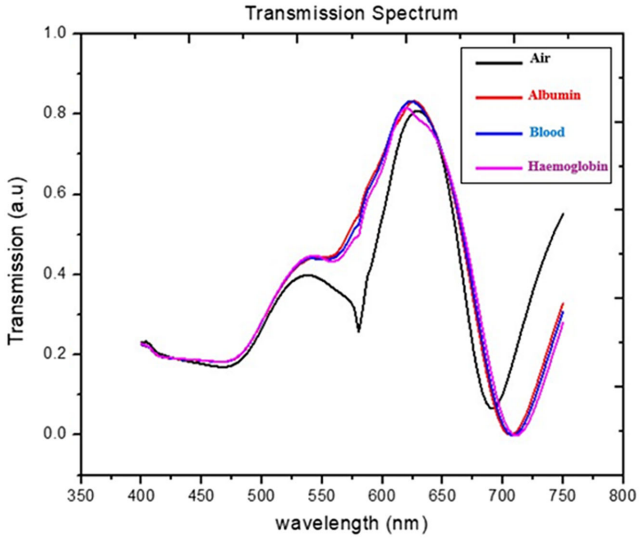

Figure 9
Normalized transmission spectrum for various analytes

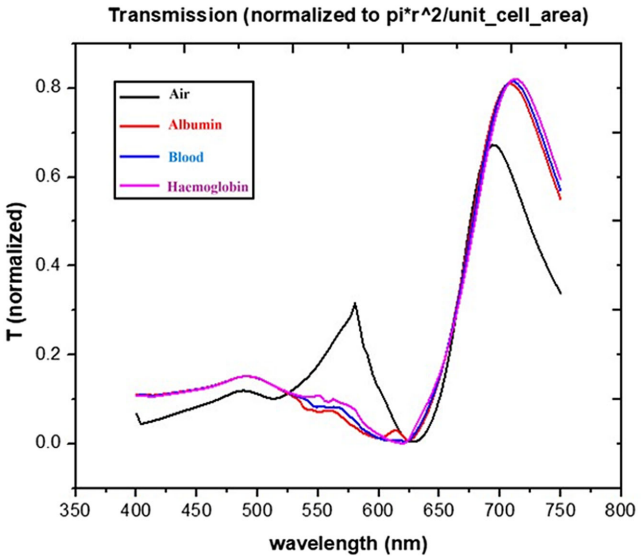

specified in Table 4. The sensitivity of the sensor is a very important parameter. The intensity interrogation method is used for finding the amplitude and frequency.

5. Conclusion

In this work, SPR-based NHA is designed, and simulation results are reported. This work also presents a detailed literature review, followed by mathematical modeling details. SPR NHA are sensitive elements used in the design and implementation of SPR sensors for use in biomedical applications. The RI-based sensor is designed using combination of SPR NHA. The material used for the thin film is gold, and the substrate is silicon dioxide. NHA is created on the gold material and illuminated by a light source with a wavelength range of 400–800 nm. The proposed sensor exhibits the highest sensitivity at a wavelength of ≈640 nm for the analyte with a RI of 1.36. The SPR NHA is showing the highest sensitivity of 298.35 nm/RIU, which is achieved for an analyte with an RI of 1.36, which is almost close to the RI of human blood. Such sensors can be used to detect various pathological parameters present in blood for the detection of various diseases.

Acknowledgments

The authors would like to acknowledge Research Centre Department of ECE, Sai Vidya Institute of Technology and Visvesvaraya Technological University (VTU), Belagavi, Karnataka, India for providing us an opportunity to carry out this research work.

Ethical Statement

This study does not contain any studies with human or animal subjects performed by any of the authors.

Conflicts of Interest

The authors declare that they have no conflicts of interest to this work.

Data Availability Statement

Data sharing is not applicable to this article as no new data were created or analyzed in this study.

Author Contribution Statement

Suryanarayana N K: Conceptualization, Methodology, Software, Validation, Formal analysis, Investigation, Data curation, Writing – original draft, Writing – review & editing, Visualization, Project administration. **Venkatesha Muniswamy:** Conceptualization, Validation, Formal analysis, Resources, Data curation, Writing – review & editing, Supervision, Project administration. **Asha K:** Conceptualization, Software, Validation, Formal analysis, Resources, Data curation, Writing – review & editing, Visualization, Supervision.

References

[1] Ahmed, T., Haque, A. N., & Talukder, M. A. (2023). Multiple features-based improved nanohole array plasmonic biosensor. *IEEE Sensors Journal*, *23*(12), 12743–12751.

[2] Chu, Y., Schonbrun, E., Yang, T., & Crozier, K. B. (2008). Experimental observation of narrow surface plasmon resonances in gold nanoparticle arrays. *Applied Physics Letters*, *93*(18), 181108.

[3] Homola, J., Yee, S. S., & Gauglitz, G. (1999). Surface plasmon resonance sensors: Review. *Sensors and Actuators B: Chemical*, *54*(1–2), 3–15.

[4] Yu, X. L., Wang, D.X., Wei, X., Ding, X., Liao, W., & Zhao, W. (2005). A surface plasmon resonance imaging interferometry for protein micro-array detection. *Sensors and Actuators B: Chemical*, *108*(1–2), 765–771.

[5] Du, G. X., Mori, T., Suzuki, M., Saito, S., Fukuda, H., & Takahashi, M. (2010). Evidence of localized surface plasmon enhanced magneto-optical effect in nanodisk array. *Applied Physics Letters*, *96*(8), 081915.

[6] Smith, E. A., & Corn, R. M. (2003). Surface plasmon resonance imaging as a tool to monitor biomolecular interactions in an array based format. *Applied Spectroscopy*, *57*(11), 320A–332A.

[7] Rich, R. L., Cannon, M. J., Jenkins, J., Pandian, P., Sundaram, S., Magyar, R., . . . , & Myszka, D. G. (2008). Extracting kinetic rate constants from surface plasmon resonance array systems. *Analytical Biochemistry*, *373*(1), 112–120.

[8] Houngkamhang, N., Vongsakulyanon, A., Peungthum, P., Sudprasert, K., Kitpoka, P., Kunakorn, M., . . . , & Srikhirin, T. (2013). ABO blood-typing using an antibody array technique based on surface plasmon resonance imaging. *Sensors*, *13*(9), 11913–11922.

[9] Salomon, A., Gordon, R. J., Prior, Y., Seideman, T., & Sukharev, M. (2012). Strong coupling between molecular excited states and surface plasmon modes of a slit array in a thin metal film. *Physical Review Letters*, *109*(7), 073002.

[10] Irannejad, M., & Cui, B. (2013). Effects of refractive index variations on the optical transmittance spectral properties of the nano-hole arrays. *Plasmonics*, *8*(2), 1245–1251.

[11] Prasad, A., Choi, J., Jia, Z., Park, S., & Gartia, M. R. (2019). Nanohole array plasmonic biosensors: Emerging point-of-care applications. *Biosensors and Bioelectronics*, *130*, 185–203.

[12] Tetz, K. A., Pang, L., & Fainman, Y. (2006). High-resolution surface plasmon resonance sensor based on linewidth-optimized nanohole array transmittance. *Optics Letters*, *31*(10), 1528–1530.

[13] Van Beijnum, F., Van Veldhoven, P. J., Geluk, E. J., de Dood, M. J., Gert, W., & Van Exter, M. P. (2013). Surface plasmon lasing observed in metal hole arrays. *Physical Review Letters*, *110*(20), 206802.

[14] Brolo, A. G., Gordon, R., Leathem, B., & Kavanagh, K. L. (2004). Surface plasmon sensor based on the enhanced light transmission through arrays of nanoholes in gold films. *Langmuir*, *20*(12), 4813–4815.

[15] Jensen, T. R., Duval, M. L., Kelly, K. L., Lazarides, A. A., Schatz, G. C., & Van Duyne, R. P. (1999). Nanosphere lithography: Effect of the external dielectric medium on the surface plasmon resonance spectrum of a periodic array of silver nanoparticles. *The Journal of Physical Chemistry B*, *103*(45), 9846–9853.

[16] Thio, T., Ghaemi, H. F., Lezec, H. J., Wolff, P. A., & Ebbesen, T. W. (1999). Surface-plasmon-enhanced transmission through hole arrays in Cr films. *Journal of the Optical Society of America B*, *16*(10), 1743–1748.

[17] Najiminaini, M., Vasefi, F., Kaminska, B., & Carson, J. J. (2012). Nano-hole array structure with improved surface plasmon energy matching characteristics. *Applied Physics Letters*, *100*(4), 043105.

[18] Singh, P. (2016). SPR biosensors: Historical perspectives and current challenges. *Sensors and Actuators B: Chemical*, *229*, 110–130.

[19] Dintinger, J., Klein, S., Bustos, F., Barnes, W. L., & Ebbesen, T. W. (2005). Strong coupling between surface plasmon-polaritons and organic molecules in subwavelength hole arrays. *Physical Review B*, *71*(3), 035424.

[20] Wei, P. K., Chou, H. L., & Fann, W. S. (2002). Optical near field in nanometallic slits. *Optics Express*, *10*(24), 1418–1424.

[21] Agrawal, A. K., Suchitta, A., & Dhawan, A. (2022). Nanostructured plasmonic chips employing nanopillar and nanoring hole arrays for enhanced sensitivity of SPR-based biosensing. *RSC Advances*, *12*(2), 929–938.

[22] Yan, W. G., Li, Z. B., & Tian, J. G. (2015). Tunable fabrication and optical properties of metal nano hole arrays. *Journal of Nanoscience and Nanotechnology*, *15*(2), 1704–1707.

[23] Gordon, R., Sinton, D., Brolo, A. G., & Kavanagh, K. L. (2008). Plasmonic sensors based on nano-holes: Technology and integration. *Micro (MEMS) and Nanotechnologies for Space, Defense, and Security II*, *6959*, 248–253.

[24] Jung, L. S., Campbell, C. T., Chinowsky, T. M., Mar, M. N., & Yee, S. S. (1998). Quantitative interpretation of the response of surface plasmon resonance sensors to adsorbed films. *Langmuir*, *14*(19), 5636–5648.

[25] Sonntag, F., Schmieder, S., Danz, N., Mertig, M., Schilling, N., Klotzbach, U., & Beyer, E. (2009). Novel lab-on-a-chip system for the label-free detection of DNA hybridization and protein-protein interaction by surface plasmon resonance (SPR). *Bioengineered and Bioinspired Systems IV*, *7365*, 227–235.

[26] Neužil, P., Campos, C. D. M., Wong, C. C., Soon, J. B. W., Reboud, J., & Manz, A. (2014). From chip-in-a-lab to lab-on-a-chip: Towards a single handheld electronic system for multiple application-specific lab-on-a-chip (ASLOC). *Lab on a Chip*, *14*(13), 2168–2176.

[27] Renaudin, A., Chabot, V., Grondin, E., Aimez, V., & Charette, P. G. (2010). Integrated active mixing and biosensing using surface acoustic waves (SAW) and surface plasmon resonance (SPR) on a common substrate. *Lab on a Chip*, *10*(1), 111–115.

[28] Kim, S., Shin, J. H., Kim, S., Yoo, S. J., Jun, B. O., Moon, C., & Jang, J. E. (2016). Geometric effects of nano-hole arrays for label free bio-detection. *RSC Advances*, *6*(11), 8935–8940.

[29] Kang, L., Zhang, Y., Gong, Q., Das, C. M., Shao, H., Poenar, D. P., . . . , & Yong, K. T. (2022). Label-free plasmonic-based biosensing using a gold nanohole array chip coated with a wafer-scale deposited WS 2 monolayer. *RSC Advances*, *12*(51), 33284–33292.

[30] Sahu, S. K., & Singh, M. (2023). Plasmonic elliptical nanohole array for on-chip human blood group detection. *IEEE Sensors Journal*, *23*(22), 27224–27230.

[31] Chen, S. H., Hsieh, W. J., Hong, Y. W., Huang, H. J., Chiang, L. M., Kao, T. S., . . . , & Chiang, H. P. (2023). Gold nanohole arrays with ring-shaped silver nanoparticles for highly efficient plasmon-enhanced fluorescence. *Results in Physics*, *51*, 106740.

[32] Miao, W., Yang, Y., Zhao, J., Zhang, H., Guo, Z., Cui, Y., . . . , & Zhu, Y. (2023). Fabrication of Au/AAO/Au nanopore arrays based on induced excitation SPPs for the fabrication of nanopores on silicon surfaces. *Materials Today Communications*, *35*, 105953.

[33] Homola, J. (2008). Surface plasmon resonance sensors for detection of chemical and biological species. *Chemical Reviews*, *108*(2), 462–493.

[34] Nikitin, P. I., Grigorenko, A. N., Beloglazov, A. A., Valeiko, M. V., Savchuk, A. I., Savchuk, O. A., . . . , & Salzer, R. (2000). Surface plasmon resonance interferometry for micro-array biosensing. *Sensors and Actuators A: Physical*, *85*(1–3), 189–193.

[35] Lee, K. L., Lee, C. W., Wang, W. S., & Wei, P. K. (2007). Sensitive biosensor array using surface plasmon resonance on metallic nanoslits. *Journal of Biomedical Optics*, *12*(4), 044023.

[36] Singh, B. K., & Hillier, A. C. (2006). Surface plasmon resonance imaging of biomolecular interactions on a grating-based sensor array. *Analytical Chemistry*, *78*(6), 2009–2018.

[37] Dostálek, J., Homola, J., & Miler, M. (2005). Rich information format surface plasmon resonance biosensor based on array of diffraction gratings. *Sensors and Actuators B: Chemical*, *107*(1), 154–161.

[38] Ashcroft, N. W., & Mermin, N. D. (1976). Electron levels in a periodic potential: General properties. In *Solid State Physics* (pp. 133–150). Saunders College.

[39] Lazareva, E. N., & Tuchin, V. V. (2018). Blood refractive index modelling in the visible and near infrared spectral regions. *Journal of Biomedical Photonics & Engineering*, *4*(1), 35–41.

How to Cite: N K, S., Muniswamy, V., & K, A. (2024). Sensitivity Analysis of SPR Nanohole Array Structure for Lab-On-Chip Application. *Journal of Optics and Photonics Research*, https://doi.org/10.47852/bonviewJOPR42021933